

Provided for non-commercial research and education use.
Not for reproduction, distribution or commercial use.



This article was published in an Elsevier journal. The attached copy is furnished to the author for non-commercial research and education use, including for instruction at the author's institution, sharing with colleagues and providing to institution administration.

Other uses, including reproduction and distribution, or selling or licensing copies, or posting to personal, institutional or third party websites are prohibited.

In most cases authors are permitted to post their version of the article (e.g. in Word or Tex form) to their personal website or institutional repository. Authors requiring further information regarding Elsevier's archiving and manuscript policies are encouraged to visit:

<http://www.elsevier.com/copyright>



Evaluation of earthquake potential and surface deformation by Differential Interferometry

Jiun-Yee Yen^{a,*}, Kun-Shan Chen^a, Chung-Pai Chang^a, Wolfgang-Martin Boerner^{a,b}

^a Center for Space and Remote Sensing Research, National Central University, No.300, Zhongda Rd., Zhongli City, Taoyuan County 320, Taiwan

^b UIC-ECE Communications, Sensing & Navigation Laboratory 900 W. Taylor St., SEL (607) W-4210, M/C 154, 60607-7018, Chicago Il, USA

Received 12 February 2007; received in revised form 11 June 2007; accepted 18 June 2007

Abstract

Uncertainties in the length of active faults and the styles of deformation often hamper the evaluation of seismic potentials in a region. In the area near Chiayi City of southwestern Taiwan, where historically there have been many strong earthquakes, complex fault and fold systems produced by regional tectonic forces and the subsequent deformation are frequently obscured by vegetation and anthropogenic effects; and therefore detailed deformation information has not been available for evaluation of the seismic potential. By stacking the results from Differential Interferometry and removing the ambiguity of interferograms using GPS data, we were able to retrieve surface deformation information about the area under consideration near Chiayi City. In our results, we found that the Meishan fault to the north of Chiayi City extended 10 km to the west of its currently documented area and served as a geological boundary separating the northern part, where sediments were thicker, from the southern part of the westward extension of the Meishan fault. Chiayi City was under active deformation by a double plunging fold with vertical uplift rate at approximately 1 cm/yr. Frequent seismicity and active deformation allowed the tectonic stress to permute between strike-slip and thrust in this area. Continuous folding of Chiayi City and episodic large earthquakes along the Meishan Fault posed a serious threat of seismic hazards in this region, and called for continuous monitoring of the area.

© 2007 Elsevier Inc. All rights reserved.

Keywords: Differential Interferometry; Earthquake; Hazard; Taiwan; Chiayi; Meishan Fault; GPS

1. Introduction

Earthquake magnitudes are known to be well correlated with the logarithms of the rupture length (Bonilla et al., 1984). Therefore, by mapping the length of fault surface rupture, it is possible to calculate the magnitudes for both past and likely future earthquakes. Traditionally, the length of a fault is generally determined by extensive field work. However, there exist many factors that affect the precise determination of the measured length of a fault rupture, such as natural erosion of the fault features and tilling of the land resulting from human activities. Since larger earthquakes occur less often, the fault trace of a large earthquake that could cause a great seismic potential is less likely to be preserved. Consequently, the exact length of the fault rupture may not be precisely mapped.

In addition to the length of surface ruptures caused by previous earthquakes, the local deformation type of a fault and the area near a fault may determine the extent of the seismic hazard as well. For example, is the fault of interest locked? Is the fault creeping and if so, how fast is it creeping? In an area with dynamic tectonic activity such as Taiwan, a locked fault implies that the regional tectonic force exerts stress in the area nearby the fault as well as the fault itself. Additionally, there could be a blind fault that is creeping actively and may induce fault related natural hazards.

Situated on the western border of the Pacific Rim of Fire, the island of Taiwan is under active surface deformation (Fig. 1) and is persistently threatened by seismic hazards. Chiayi City of southwestern Taiwan is located next to the Meishan fault (Fig. 2), which was responsible for an earthquake with high mortality that occurred in 1906 with $M_L=7.1$ (Cheng & Yeh, 2006; Omori, 1907). The earthquake resulted in thousands of deaths and many buildings were destroyed at a time when the area was still not highly populated. Historical records also show

* Corresponding author. Tel.: +886 03 422 7151x57618.

E-mail address: jyyen@csrnr.ncu.edu.tw (J.-Y. Yen).

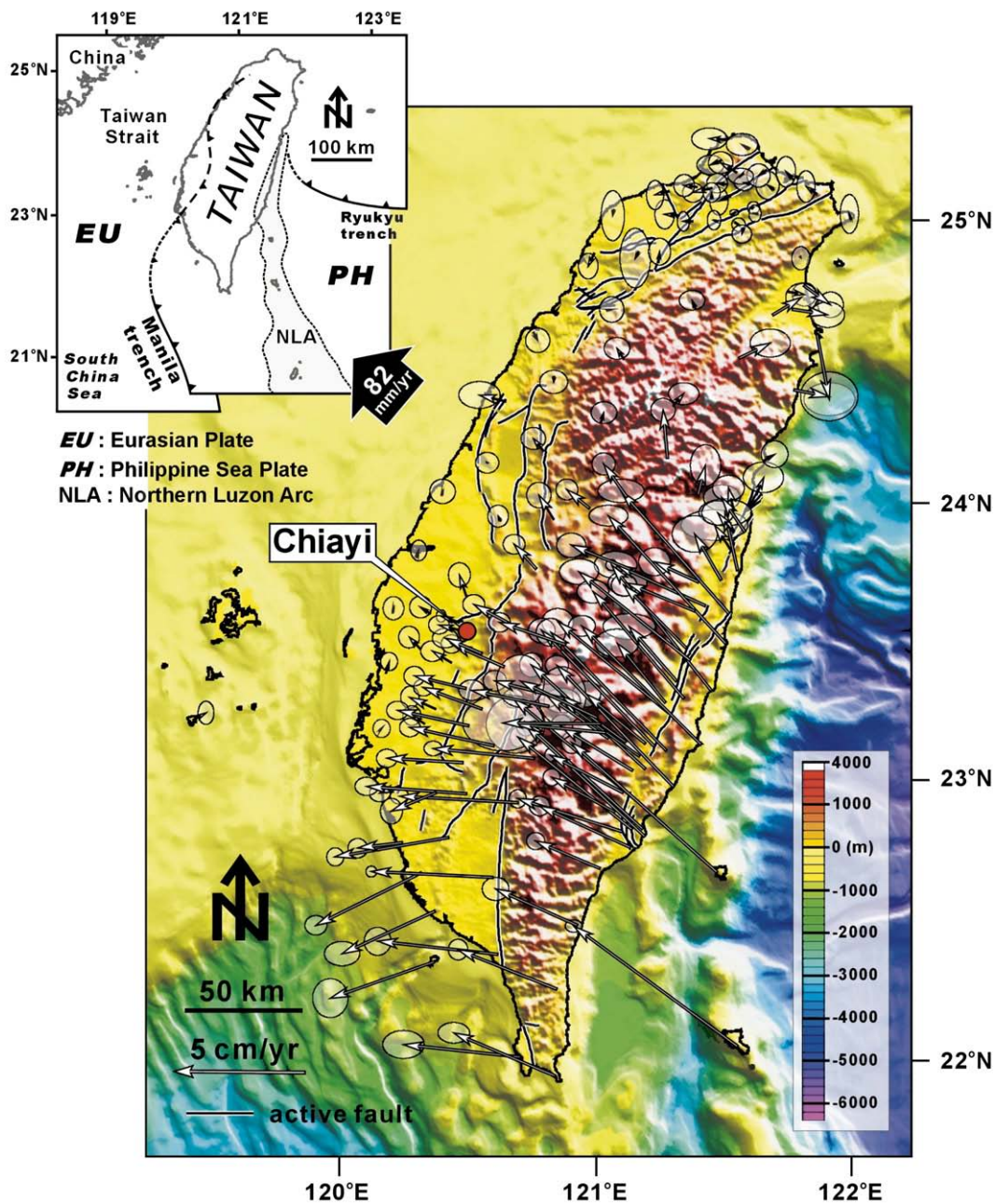


Fig. 1. Tectonic setting and velocity field of Taiwan. Philippine Sea plate is moving toward the Eurasian plate at about 82 mm/yr, creating a large compressive stress regime within the island of Taiwan. The stress is partitioned throughout the entire island as can be seen from the GPS velocity vectors. (arrows; GPS data after Yu et al., 1997). Ellipses indicated 95% confidence.

that in 1792, there was also a strong earthquake with more than 100 fatalities near Chiayi City (Omori, 1907). A century after the 1906 Meishan earthquake, the population and population density in the area is now several times higher; therefore, it is very important to evaluate the deformation type and the potential of seismic hazard in the Chiayi City area. Such knowledge would aid the government to implement warning and disaster mitigation measures for possible future earthquakes in order to minimize the pertinent damage.

Since the early 1990s, the advance of Differential Interferometry Synthetic Aperture Radar (DInSAR) technology has made it an important geodetic tool for measuring surface

deformations of both seismically related and anthropologically related deformation (Burgmann et al., 2000; Fruneau et al., 2001; Massonnet & Feigl, 1998; Schmidt & Burgmann, 2003; Zebker et al., 1994). Compared to GPS, it provides spatially much denser mapping of the deformations and it is more pervasive to visualize deformation by DInSAR. In addition, SAR images of ERS satellites cover most of the Earth surface and are archived from 1993 to present, which means that it is possible to process data related to events that occurred in the past on different time scales. Using these well-documented historical datasets, one could reach, upon applying stacking or permanent scatterer techniques, a sub-centimeter accuracy in

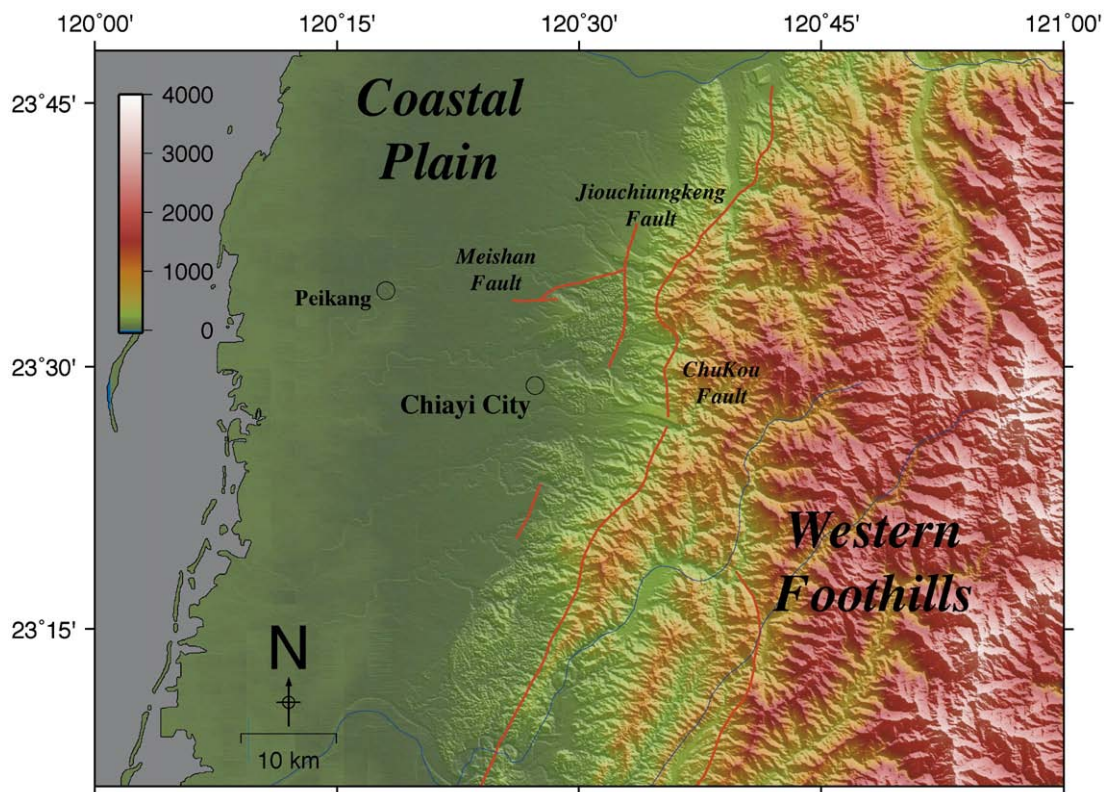


Fig. 2. Topography and faults near Chiayi City, southwestern Taiwan. The study area is located in the western Coastal Plain located west of the Western Foothills where strata were deformed and the relief is high. The two geological units are separated by the north–south trending Chukou fault. The Meishan Fault is trending approximately east–west, protruding to the west of the deformed geological unit.

measuring surface deformation. With the previously described features and advantages, DInSAR provides a very appealing alternative to other geodetic techniques.

In this paper, the main goal was to investigate the surface deformation of the region near Chiayi City and to link the observed deformation to the geological factors deduced in the area, and then to construct a geological model for explaining the observations. In order to achieve this goal, we analyzed the seismic records from the Central Weather Bureau and observed the deformation pattern using DInSAR. A total of ten radar images of track 232 and frame 3141 in descending mode acquired by the ERS-2 satellite were used (Fig. 3) to investigate the surface deformation from late 1996 to late 2000. An average deformation rate map was extracted by stacking the resulting interferograms to better understand the spatial distribution of deformation, and to trace the possible causes of the deformation. GPS data (Tsai, 2004) was also used to help resolve the ambiguity between the horizontal and vertical motions revealed in DInSAR measurements. We also evaluated the uplift potential using the horizontal motion measured by GPS, where we assumed that the conservation of volume holds and that all horizontal velocity gradients would be reflected to vertical motion. By this simple model, it is possible to look at whether the uplift potential and the uplift are equal to each other and to exploit the factors causing the physical difference between the two. It was discovered from DInSAR results that the seismogenic Meishan Fault is apparently longer than the one

currently assumed that was derived from field work mapping, and Chiayi is gently deforming as a doubly plunged fold with a fold axis plunging both to the north and to the south.

2. Background

2.1. Tectonics of Taiwan

Most of the active deformation currently taking place in the world is generally in the convergent zones such as the subduction zone in Sumatra (Acharyya, 1998; Baroux et al., 1998; Lee & Lawver, 1995; McCaffrey et al., 2000), continent–continent collisions such as the Himalaya (Chen et al., 1993; Critelli & Garzanti, 1994; Lepichon et al., 1992), and arc–continent collisions as in Taiwan (Dorsey, 1988; Suppe, 1984; Teng, 1990). Collisions between convergent plates are one of the ways to create new landmasses. The continuous convergence between plates provides energy for materials to deform within a zone of deformation. The deformation can be manifested in forms of seismicity or creeping. While collisions between continental plates such as the Indian plate and Eurasian continent can create one of the world's largest landmasses — the Himalaya, most current collisions occur in arc–continent collision types of geological settings such as Taiwan.

The island of Taiwan is located on the southeastern peripheral of the Eurasian continent between the Philippine Sea Plate and the Eurasian Plate (Fig. 1), where the Philippine

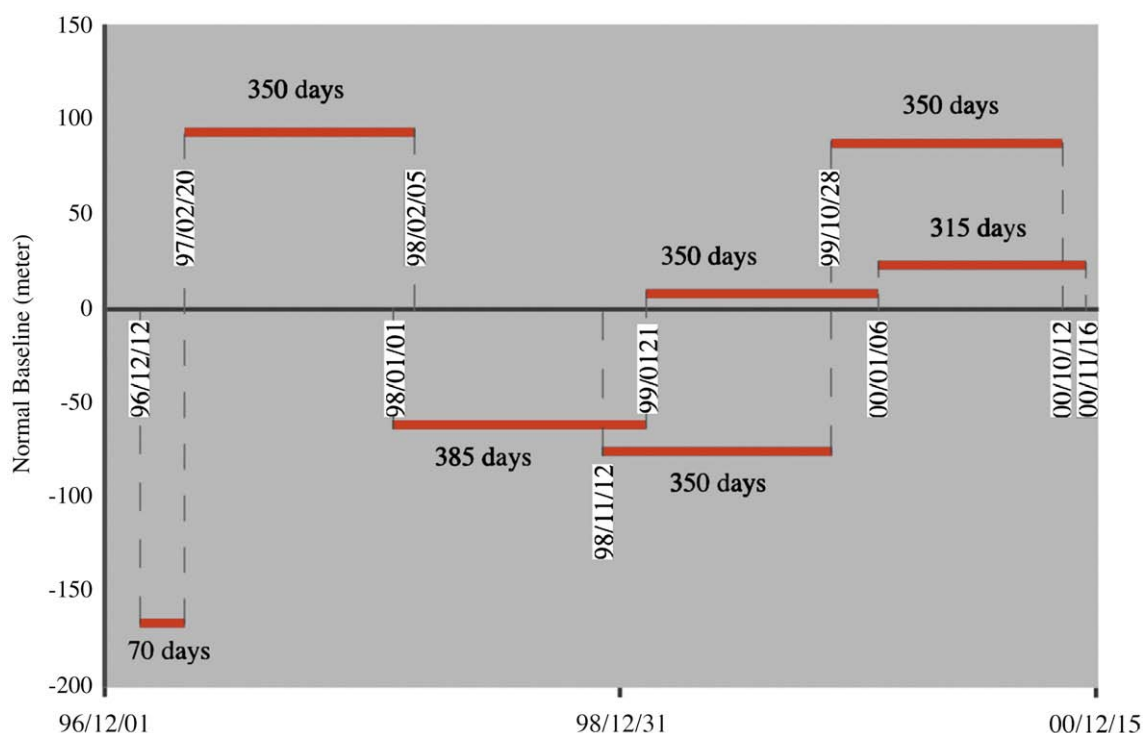


Fig. 3. ERS-2 radar images used in this paper. The perpendicular baselines of the image pairs were smaller than 150 m. During the processing of Differential Interferometry, if the DEM residuals after removing the topography were 10 m at each point, the error caused by DEM residual would be less than 0.4 cm. Radar images acquired during dry seasons were used to avoid deteriorating vegetative overburden effects of dense vegetation and farming in the study area.

Sea Plate is subducting northward in the Ryukyu trench to the north of Taiwan, while the Eurasian Plate is subducting eastward along the Manila trench to the south of Taiwan. These two tectonic plates are converging at a rate, determined geologically and geodetically, of approximately between 7 cm/yr and 8.2 cm/yr (Seno et al., 1993; Yu et al., 1997). In general, the shortening rate is higher in the eastern part of Taiwan and decreases westward. In the northern part the orogeny becomes more complex, which is reflected in the varying GPS velocity field (Fig. 1). The extreme shortening rates around the island cause extreme deformation across the island where the deformation is reflected both in the geomorphology and in seismicity. The velocity field also changes from westward moving in the central and southern part of the island to a smaller magnitude heading in various directions in the northern part of Taiwan. This could be attributed to the extension caused by the northward subducting Philippine Sea Plate and the opening of the Okinawa Trough that extends westward to onland Taiwan (Hall, 2002; Teng, 1996). The change of subduction polarity along with the fast convergent rate of the two plates caused the Luzon arc to be obducted onto the continental margin of the Eurasian continent, which resulted in the mountain building process that produced the island of Taiwan (Suppe, 1981, 1984; Teng et al., 2000). The convergence of the Eurasian Plate and the Philippine Sea Plate is partitioned throughout the island as shown in Fig. 1.

Chiayi City (Fig. 2) is surrounded by several active faults and a fold (Fuh et al., 1997; Hsu & Wey, 1983; Lin et al., 2000; Yang et al., 2006). To the north of Chiayi City, the seismogenic

Meishan fault is striking east–west. Its eastern end is terminated by the Jiouchiungkeng fault to the northeast of Chiayi City; and to the east and southeast of Chiayi City, there is the Chukou fault. The latter two faults are trending in an approximately north–south direction and constitute the frontal thrust between the western Coastal Plain and the Western Foothills. The Hsiaomei anticline is located between Chiayi City and the Jiouchiungkeng fault trending north–south, and is terminated by the Meishan fault to the north. Because of these complex structures in the surrounding area, and the high tectonic shortening rates throughout the entire island, Chiayi City is prone to seismicity and a candidate city for lurking earthquake hazards requiring thoughtful disaster mitigation measures.

2.2. Earthquake hazard

Earthquake events and potential seismic hazards are very important issues in convergent plate boundary zones such as the Himalayas, Taiwan, Japan, and New Guinea. The issues become pressing in high population density areas such as Taiwan where the occurrence of seismicity is very frequent. The seismic hazard for producing disasters is highly related to geological, physiographical, and tectonics factors such as population density, regional deformation, construction code in the affected area and soil and rock types among others; and is closely correlated with various intensities of earthquakes and shocks. Despite the existence of a clear relationship between the length of surface rupture and earthquake magnitude, there remains uncertainty in estimating past and future earthquake

magnitudes in an area nearby a known fault; hence, the seismic hazard continuously poses a serious threat of creating a major disaster for that area.

Historically, earthquakes frequently occur near Chiayi City and its surrounding area. While no major earthquake has taken place in the past few decades, around a dozen large earthquakes were reported nearby since the 17th century (Omori, 1907). Among all these recorded earthquakes, the Meishan earthquake (1906) was the most disastrous one. It caused more than 1200 casualties and wounded more than 2400 at a time when the population density was still relatively low. As this is an area with a history of frequent earthquakes that also has a long relative quiescence of massive earthquakes in recent years, it is an urgent task to investigate the currently ongoing deformation rate and deformation type in this area.

Many researchers have done a great deal of work to further improve our knowledge regarding this seismic-prone region. Omori (1907) documented the earthquakes that occurred in 1906 and other historical earthquakes that took place in the area; Cheng and Yeh (2006) went through records and reconstructed the 1906 Meishan earthquake; Yeh et al. (1984) and Yang et al. (2006) focused on fault geometry and subsurface structures in the region while others directed their attention at other properties of faults and states of stress in Taiwan (Wang & Chen, 2001; Wu & Rau, 1998). An important question raised in the area is, how does the surface move, and to what extent, in this area? Is there fault related neotectonic motion? Is there neotectonic motion that is not related to the faults in this area? How about anthropogenic surface deformation such as groundwater withdrawal for irrigation in agricultural areas and aqua-cultural regions or near urban environments? In order to answer these questions, modern geodetic methods of satellite geophysics such as DInSAR are most appropriate.

3. Data and methodology

3.1. DInSAR and ERS-2 data

In our study, ten descending orbital mode radar images of track 232 and frame 3141 acquired by the ERS-2 satellite at C-band (wavelength 5.6 cm) were used to form seven interferometric pairs (Fig. 3) that allowed us to investigate the surface deformation between late 1996 to late 2000. These interferometric processing tasks were done by implementing the two-pass method (Burgmann et al., 2000; Massonnet & Feigl, 1998) using the Diapason software developed by Centre National d'Etudes Spatiales (CNES) in 1996. Digital Elevation Model (DEM from the Aerial Survey Office of Forestry Bureau, Taiwan) of 40 m posting was used for subtracting the topography from the resulting interferograms. In particular, precise orbital data produced by the Delft Institute for Earth-Oriented Space Research (DEOS) was injected in interferometric processing to further remove the orbital uncertainties. The resulting interferograms were cleaned up by an adaptive phase filtering algorithm (Goldstein & Werner, 1998), followed by phase unwrapping using the SNAPHU program (Chen & Zebker, 2000, 2001, 2002).

3.2. Stacking

In order to obtain the average deformation rate of the study area, the unwrapped phase data was converted to annual deformation rates along the radar line-of-sight (LOS, Fig. 4) by dividing the time span of each image pair in days and multiplying by 365, subsequently divided by 2π and then multiplied by half of the wavelength of the C-band SAR used by the ERS-2 satellite. A reference point was chosen just inside Chiayi City and all deformation was re-calculated with the aid of this reference point for all the results. To stack the results together, the resulting average deformation rates derived from each image pair were added together and divided by the total number of image pairs. This process provides a way to reduce the effect of possible tropospheric delays due to atmospheric inhomogeneity and temporal variations (Wang & Liou, 2006).

3.3. GPS analyses — uplift potential

In addition to Differential Interferometry and seismicity distributions, we analyzed the GPS data currently available in this region. Many researchers have conducted GPS surveys and analyses in Taiwan (Tsai, 2004; Tsai et al., 2005; Yu et al., 1997). Tsai (2004) used data from 116 GPS stations in southwestern Taiwan to delineate the deformation in the study area. Both the campaign mode and continuous GPS were deployed between 1993 and 2003. The coseismic deformation caused by the 1999 Chi-Chi earthquake was removed from the data for evaluating the long term interseismic deformation rate in southwestern Taiwan. Our research used a comparable observation time period, and the study area was entirely covered by the GPS stations used in Tsai's research.

Since GPS has a very high resolution in the horizontal direction but a relative high uncertainty along the vertical component (3.2, 2.2, and 9.7 mm of RMS error in east–west, north–south, and vertical direction in the data used in our study), by making some simple assumptions, it is possible to calculate the theoretical vertical velocity component from the horizontal components. We defined this theoretical uplift rate as *Uplift Potential* since this value predicted the theoretical uplift rate if all the horizontal velocity changes were converted to vertical motion.

Assuming that the volume conservation is without density variations in the study area (Furbish, 1997), we may estimate the potential for uplift by the conservation equation:

$$\nabla V = 0 \quad (1)$$

where $V = (V_x, V_y, V_z)$, and V_x, V_y, V_z are velocity vectors in x , y , and z directions, respectively.

Integrating (Eq. (1)) with respect to depth (z axis), we obtain:

$$\int_0^\xi \nabla V dz = \int_0^\xi \left(\frac{\partial u}{\partial x} + \frac{\partial v}{\partial y} + \frac{\partial w}{\partial z} \right) dz = 0 \quad (2)$$

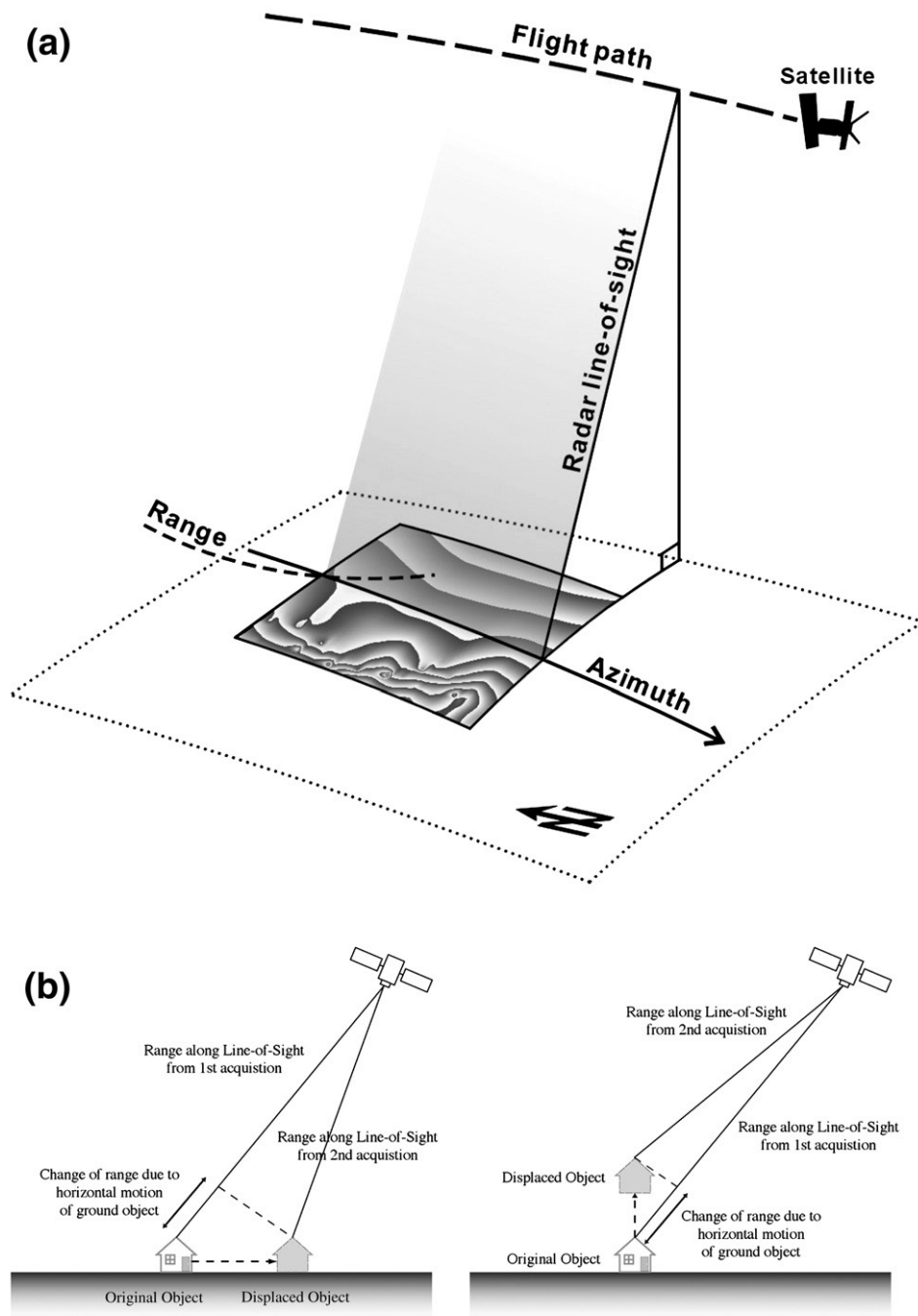


Fig. 4. (a) Satellite acquisition geometry; (b) DInSAR only measures range change along the direction of radar line-of-sight. In this special case, the horizontally displaced object has the same range change as the vertically displaced object.

where ξ is the topographic height. By noting the definition of velocity and applying the Leibniz integral rule, the following relation holds:

$$\frac{\partial}{\partial x}(\xi V_x) + \frac{\partial}{\partial y}(\xi V_y) = \frac{d\xi}{dt} \quad (3)$$

Note that the above equation has three variables, V_x , V_y , and ξ . We can then use GPS data for V_x and V_y , and solve for ξ numerically with a finite difference scheme. It is recognized that $d\xi/dt$ has the same unit as velocity, and is indeed the uplift rate

as long as the horizontal velocity gradient exists. To further reduce the uncertainties caused by marginal and boundary effects, we used the available GPS measured dataset over southwestern Taiwan (Tsai, 2004) which well covers our study area.

3.4. Ambiguity removal for DInSAR result

DInSAR is an unprecedented technique to measure the surface movement of the target area between the two image acquisitions and has been used in various settings for detecting

surface deformations (Fielding et al., 2004; Mellors et al., 2004; Rosen et al., 1996; Tomiyama et al., 2004). Differential Interferometry, as compared to GPS, measures displacements along the slant range direction instead of horizontal or vertical changes in distance (Fig. 4b). A decrease in range could imply either a vertical uplift or a horizontal motion to the east (for a descending orbital mode ERS satellite, for example). Therefore, there is ambiguity when an interferogram indicates an increase or decrease in slant range. In general, knowledge of the local geological structure may allow for eliminating most of the ambiguities, if any. However, without *a priori* knowledge, a better solution is by fusing ancillary data offered by ground truth and GPS data, as shown below.

Since the implemented DInSAR dataset is more sensitive to vertical motion due to the small incidence angle of the ERS radar satellite, while GPS generally offers better precision in horizontal motion, it is possible to project the GPS horizontal velocity field onto the radar LOS direction,

$$\begin{bmatrix} \cos\phi & -\sin\phi \\ \cos\phi\sin\theta & -\sin\phi\sin\theta \end{bmatrix} \begin{bmatrix} V_e \\ V_n \end{bmatrix} = \begin{bmatrix} V_a \\ V_l \end{bmatrix} \quad (4)$$

where ϕ is the angle between satellite ground track and the north, θ is the incident angle of the radar signal; V_e , V_n are the east and north components of GPS velocity; and V_a , V_l are the velocity components of projected GPS data in radar azimuthal and line-of-sight directions; the V_a was subsequently used to subtract the horizontal velocity field from the stacked interferogram.

4. Results

4.1. Original result (before ambiguity removal)

There were two major deformation zones that stood out and were revealed by the resulting stacked interferograms. One was near the Meishan fault and the other was in Chiayi City. Interferometric signals showed that there was a linear feature trending east–west, demonstrating active deformation in this area (Fig. 5). This east–west trending deformation zone was sub-parallel to the Meishan Fault and was principally connected to the western extension of the Meishan Fault. The slant range deformation across this deformation zone amounted to approximately 4 cm/yr. In Chiayi City a signal of deformation was observed. This deformation map indicated that the slant range deformation in Chiayi City was approximately 1 cm/yr relative to its vicinity and showed a north-northeast to south-southwest trending axis of shortening in the satellite LOS direction.

To illustrate the deformation trend, three profiles were extracted from the stacked interferogram (Fig. 5, blue diamonds), each one containing all the information about the line with 10 pixels in width. The AA' profile ran north–south across the western extension of the Meishan fault and showed a great difference of up to 4.5 cm/yr in the deformation rate between the northern and southern tip of the profile, with the northern end moving away in LOS direction. The east–west

profile BB' showed a clear uplift trend in the hub of Chiayi City, and the deformation rate decreased rapidly toward the west, while the deformation rate in the eastern part had a sharper dip than that of the western part of the profile. The signal to the east of this area was lost because of low coherence due to dense vegetation and a steeper slope. The northeast–southwestward trending CC' profile indicated a gentle uplift of 1.0 cm/yr in the center of Chiayi City compared to the north and south of the profile; the deformation rate dropped faster toward the north and more gently to the south. The peak to the north of Chiayi City in profile CC' was a curious feature, however, the profile exhibited more scattered data points near the peak compared to the data points near Chiayi City and many of the data points were masked because of the low coherence in the area. It is likely that the peak was caused by the noisy signals that passed the masking threshold.

4.2. Results after ambiguity removal

Although two deformation zones were identified near Chiayi City in the stacked interferogram, it was not possible to perceive whether the deformation was caused by horizontal motion, vertical motion, or both. Therefore, we subtracted the horizontal component from the stacked interferogram to remove this ambiguity such that the corrected deformation map included deformation contributed solely by vertical motion, and was measured in radar LOS direction (Fig. 5b).

The same profiles were also extracted from the corrected deformation map and are shown in Fig. 5a (red circles). In profile AA', the deformation rate across the extension of the Meishan Fault was approximately 3.5 cm/yr along radar LOS direction, while deformation rates in Chiayi City remained the same. This implied that no relative horizontal motion contributed to the deformation in Chiayi City.

4.3. Uplift potential

GPS data (GPS stations in Fig. 6a) of southwestern Taiwan (Tsai, 2004) was used in the model described in the previous section. The calculated result of the potential uplift rate in the study area is shown in Fig. 6b, where the warmer colors indicate positive uplift potential and cooler colors indicate negative uplift potential. By our definition (described in Section 3c), the uplift potential indicates the maximum possible uplift rate that could happen in an area if the assumptions were met. The discrepancy between the measured uplift rate (from either radar interferometry or GPS) and the uplift potential may have been caused by a localized subsidence that counterbalanced the uplift or by another mechanism that prevented uplift.

Chiayi City appeared to be an area with positive uplift potential. While this was not revealed in the GPS measured uplift rate in Fig. 6a, it was captured by the DInSAR result shown in Fig. 5. Specifically, there seemed to be two northeast–southwestward trending fold axes near Chiayi City that coincided with DInSAR observation mentioned in the previous section. One is between Station S008 to the south of Chiayi City and Station STCS to the north, and the other is between S007 to

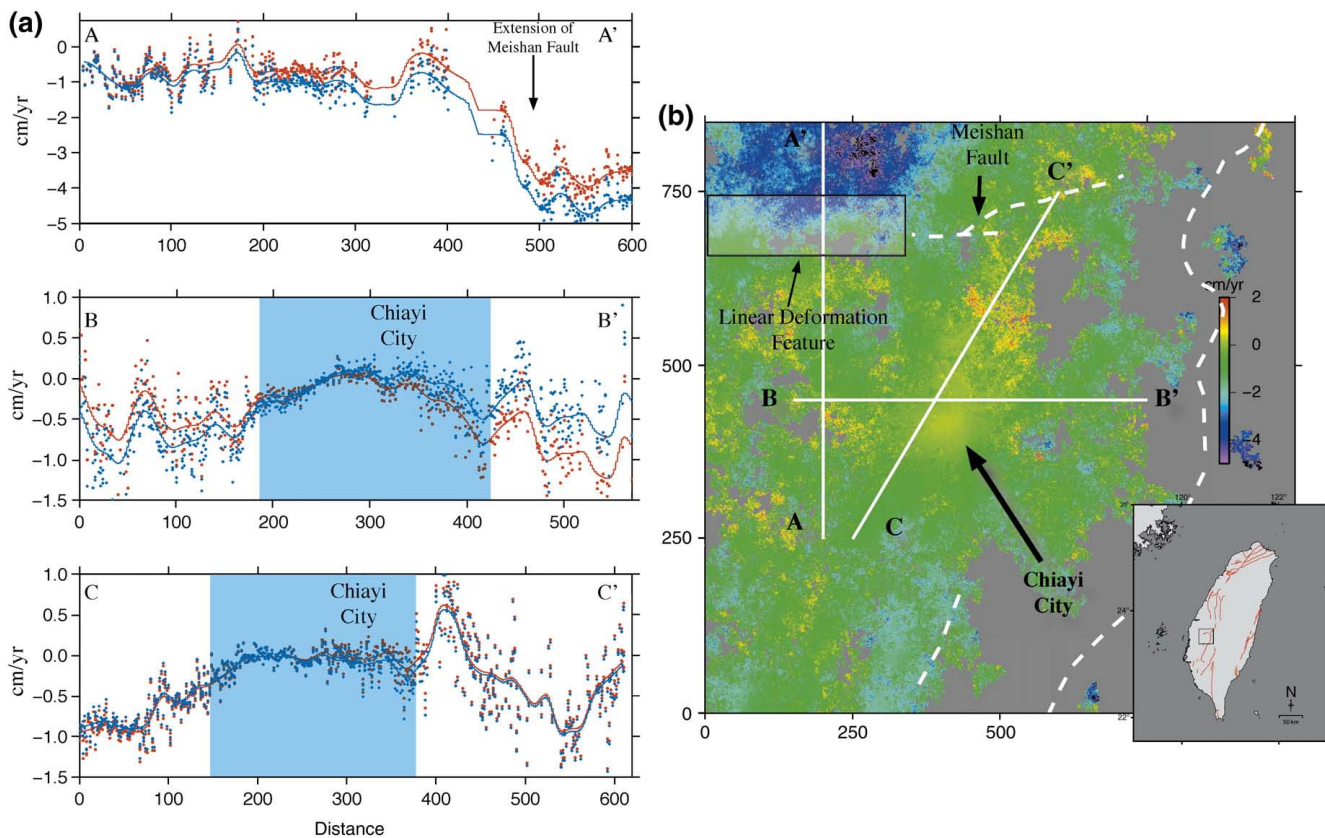


Fig. 5. Results of DInSAR analyses in the area of study. (a) Profiles extracted from both the originally stacked interferogram (marked as blue diamonds) and from results after removal of ambiguities (marked as red circles). Blue diamonds are the deformation rate of the original stacked interferogram and red circles are the deformation velocity after removal of ambiguity. Blue and red lines are the smoothed trend lines of the original signal. AA' profile originally showed 4 cm/yr difference in deformation rate across the western extension of the Meishan Fault, but became 3.5 cm/yr after removing the ambiguity. Chiayi City exhibited 1 cm/yr deformation rate against its neighboring area. Note that each profile consisted of three neighboring lines of data; therefore, each x position has ten points. Areas with low coherence showed larger degree of scattering. (b) Deformation map after removal of horizontal motion. Although the general deformation pattern is similar to the one before correcting the ambiguity, the magnitude near the Meishan fault was significantly different. A linear feature extends the seismogenic Meishan Fault to Peikang area; and Chiayi City is undergoing active deformation, too. Units in both horizontal and vertical axes are in pixel sizes (equivalent to 40 m.) Grey color indicated loss of coherence.

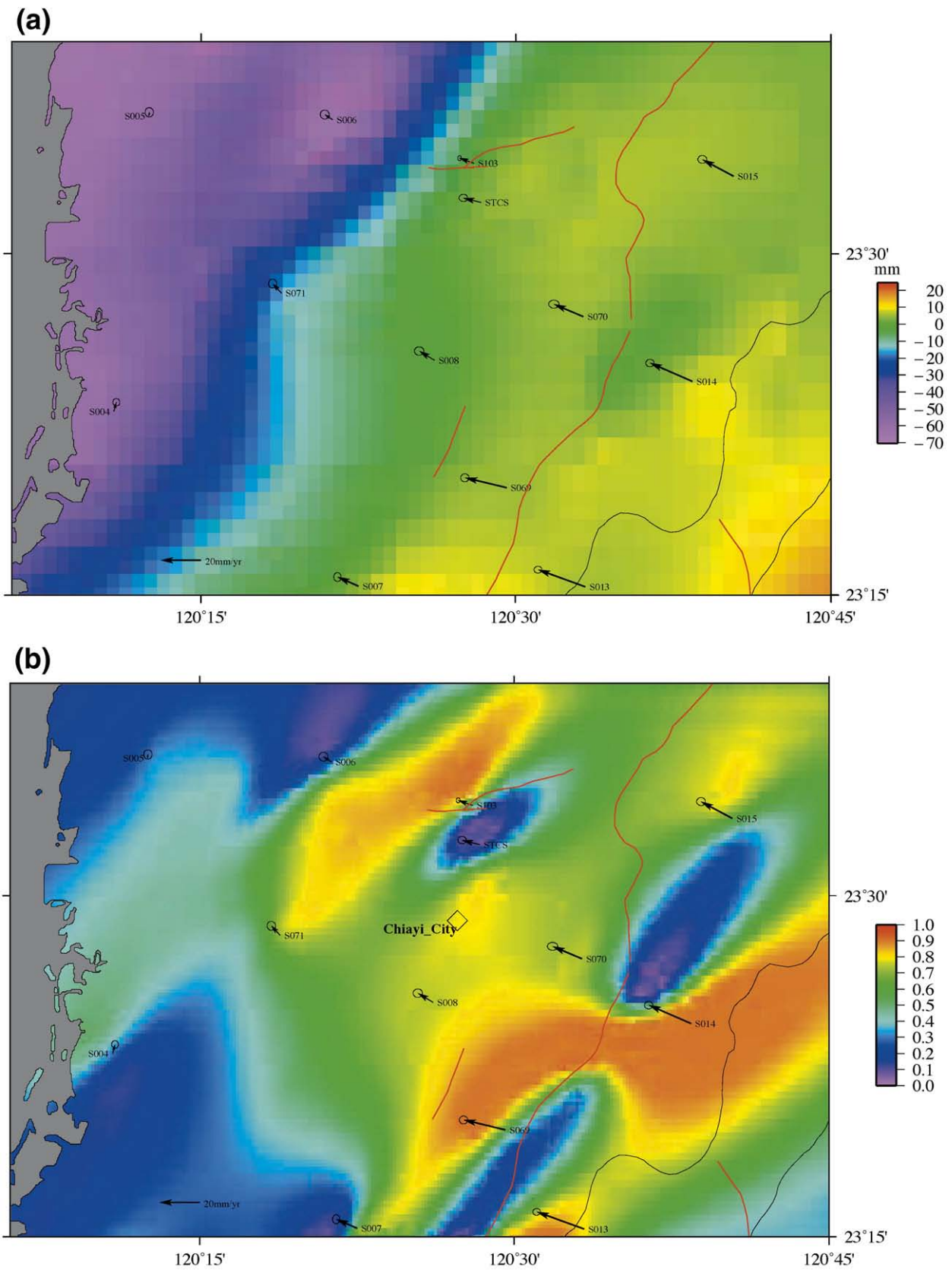


Fig. 6. Comparison of measured uplift rate from GPS and “predicted” uplift rate (uplift potential) according to our model using GPS data. Red lines indicated active faults in the area. Arrows and station names indicated the GPS data points. (a) GPS measured uplift rate (data from Tsai, 2004), Ellipses indicated 95% confidence; and (b) Uplift potential (normalized) calculated in this study. Both data exhibited higher magnitudes on the southeastern side and lower magnitudes on the northwestern side. The uplift in Chiayi City observed by DInSAR (Fig. 5b) can be seen in uplift potential, while the uplift rate measured by GPS did not capture the deformation.

the southeast of Chiayi City and S070 to the northeast that approximately coincided with the Hsiaomei anticline. In these two areas, the uplift potential and measured uplift rates were comparable. However, there was a discrepancy between the uplift potential and the measured uplift rate in the area to the west of Chiayi City to the northeast of the Station S071, although it was uncertain what contributed to this discrepancy. While our model only intended to estimate the uplift potential to the first order, it also captured the tectonic features in the area.

5. Discussion

5.1. Effect of stacking

The effect of the atmospheric phase screen (APS) for the island of Taiwan is an important issue in radar interferometry. In Taiwan, seasonal and daily changes in the atmospheric meteorological condition greatly affect the microwave propagation and reduce the accuracy of GPS positioning (Wang & Liou, 2006). If the APS presents a major disturbance in one of the radar images, then the interferogram derived from the image pair will be affected by this amount of APS, while other image pairs might not have the APS effect at all. This APS phenomenon resulted in error in the interpretation of the interferograms. Since the atmospheric conditions are different every day, they are different during each image acquisition. Therefore, theoretically, APS does correlate in time. By averaging out the interferograms over time, the resulting deformation map should exhibit less APS effect than any individual interferogram.

5.2. Effect of removing ambiguity

The stacked interferogram revealed the surface deformation in the region near Chiayi City. However, the ambiguity caused by being unable to resolve the horizontal motion against the vertical motion posed a problem for the interpretation of the interferometric result. To better interpret the interferometric result, it was essential to remove the ambiguity in the stack interferogram. Since the Global Positioning System has a very high resolution in the horizontal direction but a relative high uncertainty in the vertical component, we utilized the horizontal component of GPS data calculated by Tsai (2004), and subtracted the horizontal component from our stacked interferometric result. The resulting deformation map showed a similar deformation pattern compared to the one before correcting for the horizontal component, but it only contained the vertical component of surface deformation that was projected onto the radar LOS direction. The deformation in the western extension of the Meishan Fault, compared to the one without correction, decreased in magnitude to approximately 3.5 cm/yr across this deformation lineation. This amount of deformation indicated that in this area, the two sides of the fault are subjected to different geological conditions. The north side of this fault extension is subsiding against the southern side of the lineation. This deformation does not, however, directly link to the motion of the Meishan Fault or its western extension discovered in this study. The vertical motion manifested by the DInSAR

technique may be attributed to the combination of differences in the thickness of sedimentary strata and groundwater withdrawal in the region. In Chiayi City, in contrast to the case near the Meishan Fault, no notable difference in the magnitude of deformation was observed. Neither profile for Chiayi City exhibited significant differences as compared to the uncorrected profiles. This result also indicated that there were strike–slip motions near the Meishan fault, while very little horizontal motion was observed in Chiayi City.

5.3. Deformation of Meishan fault and Chiayi City

The study area is bounded by the Meishan fault to the north, the Jiouchungkeng fault to the northeast, and the Chukou fault to the east. The former of which is historically seismogenic and hazardous (Cheng & Yeh, 2006; Omori, 1907), while the latter is a major geological and geomorphologic boundary (Ho, 1986) between the low lying Coastal plains to the west and the late Tertiary sedimentary sequences to its east (Fig. 2). Both faults were identified as active faults by the Central Geological Survey (Lin et al., 2000). Nevertheless, DInSAR observations (Fig. 5) of this study suggested that most deformation was concentrated in two areas, Chiayi City and the western extension of the Meishan Fault.

The deformation in the western extension of the Meishan Fault was most likely induced by groundwater extraction in the area; however, the illegal and undesirable practice was not limited to the north side of the Meishan Fault but was popular in many other regions of Taiwan as well. As shown in profile CC' of Fig. 5, if the high deformation rate shown in CC' profile is tectonically related, then the Meishan fault might be more seismogenic than our general consensus claims it to be. However, from the stacked deformation map made by implementation of the GPS corrections (Fig. 6), it is clear that the surface deformation is mostly vertical rather than horizontal, which behaves very differently from that of the known right-lateral Meishan fault. It is likely that the deformation is the result of the subsidence caused by groundwater extraction and sediment compaction to the northwest of the Meishan fault, where thicker sediments are present. The reason for the asymmetry of the deformation may be due to the differential thickness of sediments caused by the Meishan Fault and its underlying structure. Yeh et al. (1984) suggested that a graben-like structure might exist in this region based on inversions of gravity survey, which would imply that to the north of the Meishan Fault, the accommodation for sediments could be higher which would explain the presence of thicker sediments. This concurred with DInSAR observations. Nevertheless, the differential deformation across this linear feature suggests that the Meishan fault extends westward for approximately another 10 km as compared to the currently mapped western termination. This result is very significant in estimating the seismic potential based on the length of the fault (Bonilla et al., 1984).

5.4. Uplift Potential and its meaning

The dimensionless uplift potential calculated from the GPS velocity with our model captured, to the first order, the regional

tectonic features, which displayed a relatively high uplift rate in the eastern half of the figure (Fig. 6). The trend in general coincides with the uplift rates measured by GPS (Fig. 6, data from Tsai, 2004). Comparison of the dimensionless uplift potential with the stacked interferogram indicated that both of them depicted the deformation within Chiayi City. This implies that to a certain degree, the deformation near Chiayi City can be explained by the velocity gradient exerted by the regional tectonic force. In other words, the convergence between the Eurasian Plate and the Philippine Sea Plate is partitioned differently within the island of Taiwan. This differential partition of deformation created the velocity gradient, which in the absence of density changes will be reflected in the vertical motion. In Chiayi City the regional tectonic force might have led to the seismic cluster approximately 10 km in depth and caused the differential velocity. This differential velocity further generates surface deformation in the form of a north–south trending fold. Carena et al. (2002) reported a 10 km deep, gently east-dipping master detachment underneath the western part of northwestern Taiwan. This in turn suggests that the seismicity below Chiayi City, which had an average depth of 14 km, is also a western extension of the master detachment in southwestern Taiwan.

In addition to the general trend, there are areas where the uplift potential does not agree with the observed uplift. The most obvious area is the very western end of the Meishan Fault where the dimensionless uplift potential exhibited a high uplift potential but current observations in GPS and DInSAR do not confirm that prediction. However, from the GPS data, we observed a significant east–west shortening between the sites to the east and to the west of this area while not much differential velocity was observed along the north–south direction. This local shortening can be expressed in either a change in local material density or a change in vertical velocity if the conservation of mass is to hold true. Hu et al. (2001a,b) combined GPS data and with a numerical model predicted an extrusion of material in southwestern Taiwan. While the GPS data in the entirety of southwestern Taiwan exhibited an increase in magnitude as the stations located farther to the south, our study area did not show this southward increase in GPS magnitude, and there was no extrusion-related structure observed in this area, either. Therefore some of these shortenings might have been converted to potential energy that was stored in the material within the area. Furthermore, the uplift potential in Chiayi City (Fig. 6b) coincided with the surface deformation observed by DInSAR (Fig. 5), while the feature could not be seen in the uplift rates measured by GPS (Fig. 6a). We attributed this lack of observation to the spatially under-sampling of GPS and its relatively poor precision in vertical direction.

5.5. Tectonic models in the region

Although the GPS survey indicated a velocity gradient near Chiayi City, a discrepancy prevailed for opposite sides of the faults between sites to the east of Chiayi City and sites to the west of it (Fig. 6). The discrepancy of the velocity shown in

Chiayi City is between 1 to 2 cm/yr. Aside from the geodetic measurements, earthquake records of Taiwan were used to illustrate the seismicity in the study area. Earthquake data from *Broadband Arrays in Taiwan for Seismology* (BATS; <http://bats.earth.sinica.edu.tw/>) were used to plot focal mechanisms in Fig. 7a and the entire Central Weather Bureau catalogues were used and earthquakes located within our study area were plotted in Fig. 7c. In our study area (Longitude 120.25–120.75° and latitude 23.25–23.80°) there were more than 900 earthquakes with magnitude smaller than $M_w=4.5$ from 1996 to 2000, with the hypocenters at a median depth of about 14 km below the surface. Although the deepest earthquake occurred at about 295 km below the surface, about 88% of the earthquakes occurred within 50 km below the surface. From inspection of Fig. 7a it is clear that many of the earthquakes near the Meishan fault are strike–slip dominant. The seismic records from the CWB in the study area showed that, during the time from 1996 to 2000 (Fig. 7b), the density of seismicity was higher immediately beneath Chiayi City than it was in areas surrounding it. Taking into account the uncertainty of the determined depth of the seismic record (Cheng et al., 1996; Wang & Shin, 1998), the seismicity seemed to congregate in a specific horizontal zone approximately 15 km below the surface. This indicated that the deformations in this area were concentrated within this limited zone of deformation.

More specifically, the focal mechanisms of the earthquakes that occurred near Chiayi City exhibited both strike–slip and thrust characteristics, whereas most earthquakes in other places are essentially thrust in nature (Fig. 7a). While Chiayi City is separated from the Western Foothills by the Chukou Fault where strata were deformed (Fig. 7b), the existence of the Meishan Fault and the abundant seismicity to the west of the Western Foothills provide evidence that the deformation zone is very active directly beneath Chiayi City. From the seismicity and the deformation map derived from DInSAR, the active folding in Chiayi City and the seismicity clustered at the depth of 15 km are likely correlated (Fig. 7c), whereas the Meishan Fault and its western extension are a major boundary, separating different geological conditions while also acting as a strike–slip fault.

The deformation and the seismicity near Chiayi City raise an interesting question. Why did the deformation take place near Chiayi City while to the north and south of Chiayi City, no similar deformation is occurring? In addition, why did the deformation occur to the west of the major deformation zone, i.e. the Western Foothills? Why did it occur in the form of a strike–slip fault near the Meishan Fault and as a thrust faulting beneath Chiayi City, which is just less than 10 km away from the Meishan Fault? The continuing convergence between the Eurasian Plate and the Philippine Sea Plate has been exerting stress across the entire island of Taiwan. The stress was mostly absorbed in the eastern part of Taiwan which was highly deformed. As the Luzon arc is approaching the Eurasian continent at an angle, the deformation in Taiwan is propagating both southward and westward (Byrne, 1998; Suppe, 1984). While the stress remains, σ_2 and σ_3 could be disturbed by local geological settings and could cause stress permutation. The

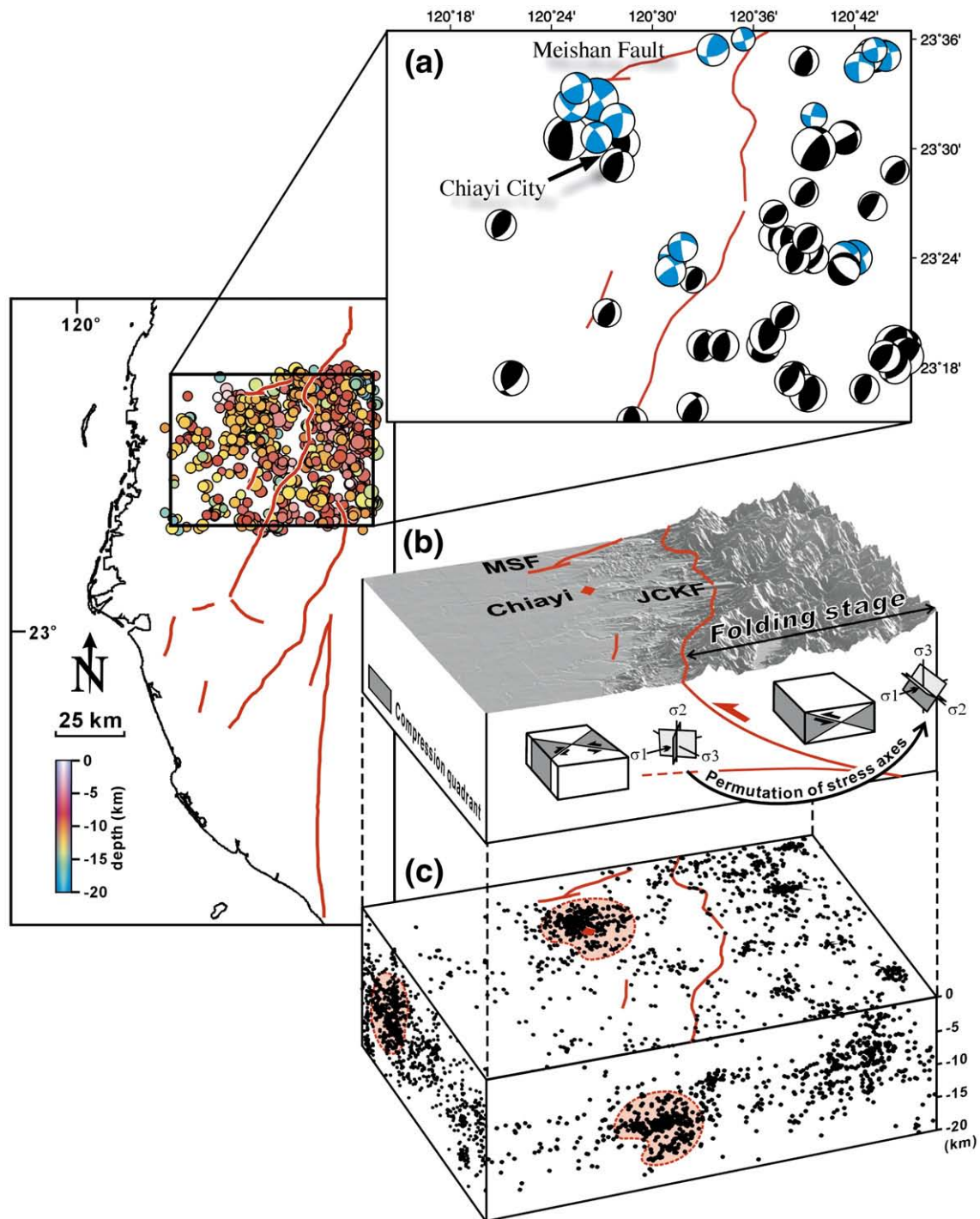


Fig. 7. Earthquakes near Chiayi City and tectonic explanation of deformation pattern. From top to bottom: (a) Focal mechanisms of earthquakes near Chiayi City (1995–2006, data from BATS). Strike-slip types of earthquakes (in blue) were closer to the Meishan Fault and reverse type of earthquakes (black) were farther away from the fault. (b) Earthquakes near Chiayi City generally occurred at about 15 km in depth. (c) The study area exhibited two stress regimes, strike-slip stress near the Meishan Fault and thrusting away from the Meishan fault, under the single dominant far-field stress resulting from the convergence between the Eurasian plate and the Philippine Sea plate.

exerting stress in this area is causing the area near Chiayi City to shorten. This can be clearly seen from the folding in Chiayi City and the dominant thrusting seismicity caused by a blind thrust under Chiayi City. A similar stress regime with greater scale can be seen in the area immediately east of the Chukou Fault, where the entire Western Foothills are shortening. However, since the

density and the depth distribution of the seismicity near Chiayi City appeared to be very local, the congregation of seismicity underneath Chiayi City does not seem to extend much farther to the north and the south. Furthermore, the seismicity and the plane on which it congregated did not appear to reach the surface, and no fault system seemed to connect to this active

deformation zone. Therefore, as the stress buildup continues until the critical point, the stored energy could be released and could be slipping along the nearby Meishan Fault, which could be disastrous, as the Meishan Fault usually exhibits little displacement.

6. Conclusions

From this study we found that stacked interferograms provide an effective means for reducing the effects of the atmospheric phase delay in the resulting deformation map, which substantially improves its accuracy. Since the deformation map derived from DInSAR contains signals that are ambiguous in actual vertical surface motion and horizontal surface motion, removing the ambiguity becomes important in an area in which both horizontal and vertical motions might contribute significant amounts of displacement. Furthermore, the high spatial sampling of DInSAR revealed more subtle and small scale deformation information compared to the result from GPS, in particular deformation in vertical direction. By removing the ambiguity using the horizontal components of GPS velocity field of the identical time period, the vertical deformation velocity near Chiayi City was retrieved.

Combining the GPS and DInSAR observations with a simple model, it was revealed that the western end of the Meishan Fault was actively deforming, and this linear deformation was clearly connected to the Meishan Fault. In other words, the Meishan Fault extends another 10 km to the west of the currently documented location. While there was no surface rupture in the area, the underlying fault clearly served as a geological boundary separating different deformation velocity to the north and south of the fault, respectively. This finding conformed with the report by Omori (1907) that to the west of the surface rupture caused by the 1906 Meishan earthquake, there were sand spills resulting from this earthquake, although there was no surface rupture in this area. Coupled with DInSAR observations, we concluded that this western extension of the Meishan Fault should be regarded as the Meishan Fault itself. Chiayi City was actively deforming as a double plunging fold. This deformation appeared to be very local and did not extend very far to the north or to the south. The continuing shortening could store potential energy and induce a large earthquake nearby.

The DInSAR observations in this study, the GPS measurements coupled with our simple model, and the seismicity in the area near Chiayi City all indicated that this region was under active deformation during the time of observation. The continuous deformation of Chiayi City along with the historically episodic seismic hazards that occurred along the Meishan Fault, demands that more attention be directed to the active deformation and the implied seismic potential in this region.

Acknowledgment

This study was funded by National Science Council under the grant NSC95-2745-M-008-008.

References

- Acharyya, S. K. (1998). Break-up of the Greater Indo-Australian Continent and accretion of blocks framing South and East Asia. *Journal of Geodynamics*, *1*, 149–170.
- Baroux, E., Avouac, J. P., Bellier, O., & Sebrier, M. (1998). Slip-partitioning and fore-arc deformation at the Sunda Trench, Indonesia. *Terra Nova*, *3*, 139–144.
- Bonilla, M. G., Mark, R. K., & Lienkaemper, J. J. (1984). Statistical relations among earthquake magnitude, surface rupture length, and surface fault displacement. *Bulletin of the Seismological Society of America*, *74*, 2379–2411.
- Burgmann, R., Rosen, P. A., & Fielding, E. J. (2000). Synthetic aperture radar interferometry to measure Earth's surface topography and its deformation. *Annual Review of Earth and Planetary Sciences*, *28*, 169–209.
- Byrne, T. (1998). Pre-collision kinematics and a possible modern analog for the Lichi and Kenting Mélanges, Taiwan. *Journal of the Geological Society of China*, *41*, 535–550.
- Carena, S., Suppe, J., & Kao, H. (2002). Active detachment of Taiwan illuminated by small earthquakes and its control of first-order topography. *Geology*, *10*, 935–938.
- Chen, C. W., & Zebker, H. A. (2000). Network approaches to two-dimensional phase unwrapping: Intractability and two new algorithms. *Journal of the Optical Society of America. A*, *17*, 401–414.
- Chen, C. W., & Zebker, H. A. (2001). Two-dimensional phase unwrapping with use of statistical models for cost functions in nonlinear optimization. *Journal of the Optical Society of America. A*, *18*, 338–351.
- Chen, C. W., & Zebker, H. A. (2002). Phase unwrapping for large SAR interferograms: Statistical segmentation and generalized network models. *IEEE Transactions on Geoscience and Remote Sensing*, *40*, 1709–1719.
- Chen, Y., Cogne, J. P., Courtillot, V., Tapponnier, P., & Zhu, X. Y. (1993). Cretaceous Paleomagnetic results from Western Tibet and tectonic implications. *Journal of Geophysical Research-Solid Earth*, *B10*, 17981–17999.
- Cheng, S. N., & Yeh, Y. T. (2006). Historical perspective of the Meishan Earthquake. *Conference in Commemoration of 100th Anniversary of the 1906 Meishan Earthquake, Taiwan*.
- Cheng, S. N., Yeh, Y. T., Huang, W. G., Shin, T. T., & Chang, G. S. (1996). The catalogue of Taiwan Earthquakes, 1989–1995. *Report of the Central Weather Bureau Report* (pp. 105).
- Crittelli, S., & Garzanti, E. (1994). Provenance of the Lower Tertiary Murree Redbeds (Hazara-Kashmir Syntaxis, Pakistan) and initial rising of the Himalayas. *Sedimentary Geology*, *3–4*, 265–284.
- Dorsey, R. J. (1988). Provenance evolution and unroofing history of a modern arc-continent collision—evidence from petrography of Plio-Pleistocene Sandstones, Eastern Taiwan. *Journal of Sedimentary Petrology*, *58*, 208–218.
- Fielding, E. J., Wright, T. J., Muller, J., Parsons, B. E., & Walker, R. (2004). A seismic deformation of a fold-and-thrust belt imaged by synthetic aperture radar interferometry near Shahdad, Southeast Iran. *Geology*, *7*, 577–580.
- Fruneau, B., Pathier, E., Raymond, D., Deffontaines, B., Lee, C., Wang, H., et al. (2001). Uplift of Tainan Tableland (SW Taiwan) revealed by SAR interferometry. *Geophysical Research Letters*, *28*, 3071–3074.
- Fuh, S. C., Liu, C. S., Lundberg, N., & Reed, D. L. (1997). Strike-slip faults offshore Southern Taiwan: Implications for the oblique arc continent collision processes. *Tectonophysics*, *1–3*, 25–39.
- Furbish, D. J. (1997). *Fluid physics in geology: An introduction to fluid motions on Earth's surface and within its crust*. New York: Oxford University Press, Inc.
- Goldstein, R., & Werner, C. (1998). Radar interferogram filtering for geophysical applications. *Geophysical Research Letters*, *21*, 4035–4038.
- Hall, R. (2002). Cenozoic geological and plate tectonic evolution of SE Asia and the SW Pacific: Computer based reconstructions, model and animations. *Journal of Asian Earth Sciences*, *4*, 353–431.
- Ho, C. S. (1984). A Synthesis of the Geologic Evolution of Taiwan, Geodynamics of the Eurasia-Philippine Sea plate boundary plate boundary. Taipei, Taiwan: Mar. 28–30, 1984. *Tectonophysics*, vol. 125. (pp. 1–16).
- Hsu, C. Y., & Wey, S. K. (1983). Structural geology in the Chiayi Foothills, Taiwan. *Petroleum Geology of Taiwan*, *19*, 17–28.

- Hu, J. -C., Angelier, J., Homberg, C., Lee, J. C., & Chu, H. T. (2001a). Three-dimensional modeling of the behavior of the oblique convergent boundary of Southeast Taiwan: Friction and strain partitioning. *Tectonophysics*, 333, 261–276.
- Hu, J. -C., Yu, S. B., Angelier, J., & Chu, H. T. (2001b). Active deformation of Taiwan from GPS measurements and numerical simulations. *Journal of Geophysical Research-Solid Earth*, B2, 2265–2280.
- Lee, T. Y., & Lawver, L. A. (1995). Cenozoic plate reconstruction of Southeast Asia. *Tectonophysics*, 251, 85–138.
- Lepichon, X., Fournier, M., & Jolivet, L. (1992). Kinematics, topography, shortening, and extrusion in the India–Eurasia collision. *Tectonics*, 6, 1085–1098.
- Lin, C. -W., Chang, H. -C., Lu, S. -T., Shih, T. -S., & Huang, W. -J. (2000). *An introduction to the active faults of Taiwan*, 2nd Edition : Central Geological Survey, Ministry of Economic Affairs.
- Massonnet, D., & Feigl, K. L. (1998). Radar interferometry and its application to changes in the Earth's surface. *Reviews of Geophysics*, 36, 441–500.
- McCaffrey, R., Zwick, P. C., Bock, Y., Prawirodirdjo, L., Genrich, J. F., Stevens, C. W., et al. (2000). Strain partitioning during oblique plate convergence in Northern Sumatra: Geodetic and seismologic constraints and numerical modeling. *Journal of Geophysical Research-Solid Earth*, B12, 28363–28376.
- Mellors, R. J., Magistrale, H., Earle, P., & Cogbill, A. (2004). Comparison of four moderate-size earthquakes in Southern California using seismology and InSAR. *Bulletin of the Seismological Society of America*, 6, 2004–2014.
- Omori, F. (1907). Preliminary note on the Formosa Earthquake of March 17, 1906. *Bulletin of Imperial Earthquake Investigation Committee*, 1, 53–69.
- Rosen, P. A., Hensley, S., Zebker, H. A., Webb, F. H., & Fielding, E. J. (1996). Surface deformation and coherence measurements of Kilauea Volcano, Hawaii, from Sir-C radar interferometry. *Journal of Geophysical Research-Planets*, E10, 23109–23125.
- Schmidt, D. A., & Burgmann, R. (2003). Time-dependent land uplift and subsidence in the Santa Clara Valley, California, from a large interferometric synthetic aperture radar data set. *Journal of Geophysical Research-Solid Earth*, B9 (p.-).
- Seno, T., Stein, S., & Gripp, A. E. (1993). A model for the motion of the Philippine Sea Plate consistent with Nuvel-1 and geological data. *Journal of Geophysical Research, B, Solid Earth and Planets*, 98, 17,941–17,948.
- Suppe, J. (1981). Mechanics of mountain building and metamorphism in Taiwan. *Memoir of the Geological Society of China*, 4, 67–89.
- Suppe, J. (1984). Kinematics of arc-continent collision, flipping of subduction, and back-arc spreading near Taiwan. *Memoir of the Geological Society of China*, 6, 21–33.
- Teng, L. S. (1990). Geotectonic evolution of late Cenozoic arc-continent collision in Taiwan. *Tectonophysics*, 183, 57–76.
- Teng, L. S. (1996). Extensional collapse of the Northern Taiwan Mountain Belt. *Geology*, 10, 949–952.
- Teng, L. S., Lee, C. T., Tsai, Y. B., & Hsiao, L. Y. (2000). Slab breakoff as a mechanism for flipping of subduction polarity in Taiwan. *Geology*, 2, 155–158.
- Tomiyama, N., Koike, K., & Omura, M. (2004). Detection of topographic changes associated with volcanic activities of Mt. Hosscho using D-InSAR. *Monitoring of Changes Related to Natural and Manmade Hazards Using Space Technology*, vol. 3. (pp. 279–283).
- Tsai, M. -C. (2004). *On GPS time series analysis of Southwestern Taiwan and crustal deformation model* (pp. 105). Institute of Geophysics.
- Tsai, M. -C., Yu, S. -B., Chen, H., Kuo, L., & Hsu, Y. (2005). Modeling studies of crustal deformation in the fold and thrust belt of Southwestern Taiwan. *Eos, Transactions of the American Geophysical Union*, 86(52) (p. Abstract G53A–0873).
- Wang, W. H., & Chen, C. H. (2001). Static stress transferred by the 1999 Chi-Chi, Taiwan, Earthquake: Effects on the stability of the surrounding fault systems and aftershock triggering with a 3D fault-slip model. *Bulletin of the Seismological Society of America*, 5, 1041–1052.
- Wang, C. S., & Liou, Y. A. (2006). A study on the relationship between seasonal variation and positioning accuracy by GPS. *Journal of Photogrammetry and Remote Sensing*, 11, 191–200.
- Wang, C. Y., & Shin, T. C. (1998). Illustrating 100 years of Taiwan seismicity. *Terrestrial Atmospheric and Oceanic Sciences*, 9, 589–614.
- Wu, F. T., & Rau, R. J. (1998). Seismotectonics and identification of potential seismic source zones in Taiwan. *Terrestrial Atmospheric and Oceanic Sciences*, 4, 739–754.
- Yang, K. -M., Liang, S. C., Huang, S. T., Wu, M. S., Wu, R. C., & Ting, H. S. (2006). Fault geometry evolution in Western Taiwan near Peikang Basement High. *Conference in Commemoration of 100th Anniversary of the 1906 Meishan Earthquake, Taiwan*.
- Yeh, Y. -H., Wang, W. -H., Yen, H. -Y., & Tsai, Y. -B. (1984). Subsurface structures in the Mingsiung-Meishan area, Southwestern Taiwan from gravity anomaly data. *Bulletin of the Institute of Earth Sciences. Bulletin of the Institute of Earth Sciences, Academia Sinica*, vol. 4. (pp. 101–116).
- Yu, S. B., Chen, H. Y., & Kuo, L. C. (1997). Velocity field of GPS stations in the Taiwan area. *Tectonophysics*, 274, 41–59.
- Zebker, H. A., Rosen, P. A., Goldstein, R. M., Gabriel, A., & Werner, C. L. (1994). On the derivation of coseismic displacement-fields using differential radar interferometry — the Landers Earthquake. *Journal of Geophysical Research-Solid Earth*, B10, 19617–19634.